Vanadyl Oxalatophosphate Compounds $(C_2H_{10}N_2)[VO(HPO_4)]_2(C_2O_4)$ and $(CH_6N_3)_2[[VO(HPO_4)]_2(C_2O_4)$ and Their Thermal Transformation to $(VO)_2P_2O_7$ via $VOHPO_4$

Junghwan Do, Ranko P. Bontchev, and Allan J. Jacobson*

Department of Chemistry, University of Houston, Houston, Texas 77204-5641

Received January 18, 2001. Revised Manuscript Received April 25, 2001

The vanadyl oxalatophosphates $(C_2H_{10}N_2)[VO(HPO_4)]_2(C_2O_4)$, **1**, and $(CH_6N_3)_2[VO(HPO_4)]_2(C_2O_4)$, **2**, have been synthesized hydrothermally and characterized by a combination of techniques including infrared spectroscopy, single-crystal/powder X-ray diffraction, scanning/transmission electron microscopy, thermogravimetric analysis, and magnetic susceptibility measurements. The structures of **1** and **2** contain the same type of $\{[VO(HPO_4)]_2(C_2O_4)\}^{2-}$ layer, including both oxalate and phosphate anions coordinated to vanadium cations, as found in the previously reported $(NH_4)_2[VO(HPO_4)]_2(C_2O_4)\cdot H_2O$. Above ∼550 °C, **1** and **2** transform to $(VO)_2P_2O_7$, the catalyst for the oxidation of butane to maleic anhydride. An intermediate phase with the composition $VOHPO_4$ is observed in the decomposition reactions. Crystal data: (**1**) triclinic, space group $P\bar{1}$ (no. 2); $a = 6.3595(7)$ Å, $b = 6.6236(7)$ Å, $c = 9.224(1)$ Å, $\alpha = 98.216(2)^o$, $\beta = 108.128(2)^o$, $\gamma = 100.672(2)^o$, $V = 354.42(7)$ Å^3, $Z = 1$; (**2**) triclinic, space group $P1$ (no. 2); $a = 6.3825(8)$ Å, $b = 7.8877(9)$ Å, $c = 9.202(1)$ Å, $\alpha = 66.602(2)^o$, $\beta = 71.757(2)^o$, $\gamma = 79.821(2)^o$, $V = 403.07(8)$ Å^3, $Z = 1$.

Introduction

Vanadyl pyrophosphate, $(VO)_2P_2O_7$, is an active and selective catalyst for the oxidation of butane to maleic anhydride.[1−4] The catalyst is prepared in its optimum form by the topotactic transformation of hydrated layered vanadium hydrogen phosphates, such as the hemihydrate $VOHPO_4\cdot 0.5H_2O$.[5−8] The topotactic decomposition preserves the precursor morphology and increases the area of the crystal faces that are thought to be responsible for the catalyst activity and selectivity. Some groups have suggested the presence of an amorphous intermediate in the transformation,[9,10] but others consider this to be unlikely.[6,7] Strain and domain size effects do, however, cause significant line broadening in X-ray diffraction patterns of samples annealed for short times just above the precursor decomposition temperature.[7,8,11] The disorder has been interpreted as arising from stacking faults that are introduced when the layers become cross-linked on the formation of the pyrophosphate groups.[8]

In this paper, we describe the synthesis and characterization of two new vanadyl oxalatophosphate compounds ($(C_2H_{10}N_2)[VO(HPO_4)]_2(C_2O_4)$, **1,** and $(CH_6N_3)_2[VO(HPO_4)]_2(C_2O_4)$, **2,** containing the same type of $\{[VO(HPO_4)]_2(C_2O_4)\}^{2-}$ layer previously found in $(NH_4)_2[VO(HPO_4)]_2(C_2O_4)\cdot H_2O$.[12] The thermal decomposition reactions of the two compounds give a previously unreported form of vanadyl hydrogen phosphate, $VOHPO_4$, and provide an alternate route to $(VO)_2P_2O_7$ catalysts.

Experimental Section

Synthesis. Compound **1** was synthesized by a two-step reaction. In the first step 17.4 g of V_2O_5 (0.0957 mol, Aldrich, 99%) was slowly added to a mixture of 18.12 g of oxalic acid (0.2012 mol, Aldrich, 98%), 34.6 mL of H_3PO_4 (0.5080 mol, Aldrich, 99.99%, 85 wt % solution in H_2O), and 150 mL of distilled water at 70 °C. The solution was heated overnight at ∼100 °C. At this point no crystallization had occurred. The resulting blue solution (solution A) was used further as a reagent for the second step of the synthesis. This synthesis is based on the results of a systematic investigation of the formation of vanadyl phosphate hydrates by D. Fratzky et al.[13] In the second step, **1** was prepared by heating 5 mL of solution A and 0.143 mL of ethylenediamine (2.1 mmol, Aldrich, 99%)

* To whom correspondence should be addressed. Phone: (713) 743-2785. Fax: (713) 743-2787. E-mail: ajjacob@uh.edu.

(1) Centi, G.; Trefiro, F.; Ebner, J. R.; Franchetti, V. M. *Chem. Rev.* **1988**, *88*, 55.
(2) Sleight, A. W. *Catal. Today* **1987**, *1*, 347.
(3) Horowitz, H. S.; Blackstone, C. M.; Sleight, A. W.; Teufer, G. *Appl. Catal.* **1988**, *38*, 193.
(4) Bordes, E. *Catal. Today* **1987**, *1*, 499.
(5) Bordes, E.; Courtine, P.; Johnson, J. W. *J. Solid State Chem.* **1984**, *55*, 270.
(6) Johnson, J. W.; Johnston, D. C.; Jacobson, A. J.; Brody, J. F. *J. Am. Chem. Soc.* **1984**, *106*, 8123.
(7) Nguyen, P. T.; Sleight, A. W.; Roberts, N.; Warren, W. W. *J. Solid State Chem.* **1996**, *122*, 259.
(8) Torardi, C. C.; Li, Z. G.; Horowitz, H. S.; Liang, W.; Whangbo, M.-H. *J. Solid State Chem.* **1995**, *119*, 349.
(9) Amorós, P.; Ibáñez, R.; Beltrán, A.; Beltrán, D.; Fuertes, A.; Gomez-Romero, P.; Hernandez, E.; Rodriguez-Carvajal, J. *Chem. Mater.* **1991**, *3*, 407.
(10) Sananes, M. T.; Tuel, A.; Hutchings, G. J.; Volta, J. C. *J. Catal.* **1994**, *148*, 395.
(11) Johnston, D. C.; Johnson, J. W. *Chem. Commun.* **1985**, 1720.
(12) Do, J.; Bontchev, R. P.; Jacobson, A. J. *Inorg. Chem.* **2000**, *39*, 3230.
(13) Fratzky, D.; Gotze, Th.; Worzala, H.; Meisel, M. *Mater. Res. Bull.* **1998**, *33*, 635.

10.1021/cm010043u CCC: $20.00
Published on Web 07/10/2001

Table 1. Crystallographic Details for 1 and 2

	1	2
formula mass, amu	475.96	532.02
space group	$P\bar{1}$ (no. 2)	$P\bar{1}$ (no. 2)
a, Å	6.3595(7)	6.3825(8)
b, Å	6.6236(7)	7.8877(9)
c, Å	9.2245(10)	9.2022(11)
α, deg	98.216(2)	66.602(2)
β, deg	108.128(2)	71.757(2)
γ, deg	100.672(2)	79.821(2)
V, Å^3	354.42(7)	403.07(8)
Z	1	1
T, K	293(2)	293(2)
λ, Å	0.71073	0.71073
ρ_{calcd} g/cm^3	2.225	2.192
μ, cm^{-1}	16.30	14.50
abs correction[a]	empirical	empirical
$F(000)$	236	266
cryst size, mm^3	0.10 × 0.10 × 0.07	0.12 × 0.02 × 0.02
2θ limits, deg	$5 \le 2\theta \le 57$	$5 \le 2\theta \le 52$
no. of all data	2205	2233
no. of unique data	1530	1504
no. of variables	129	151
goodness-of-fit	1.113	1.099
R^b	0.0321	0.0449
$R_w^{c,d}$	0.0791[c]	0.1091[d]
$(\Delta\rho)_{max}$, $(\Delta\rho)_{min}$, e/Å^3	0.729, 0.411	0.573, 0.439

[a] The program SADABS was used for the absorption correction. [b] $R = \sum||F_o| - |F_c|/\sum|F_o|$ (based on reflections with $I > 2\sigma(I)$). [c] $R_w = [\sum w(|F_o| - |F_c|)^2/\sum w|F_o|^2]^{1/2}$; $w = 1/[\sigma^2(F_o^2) + (0.0298P)^2 + 0.58P]$; $P = [\max(F_o^2, 0) + 2F_c^2]/3$ (all data). [d] $R_w = [\sum w(|F_o| - |F_c|)^2/\sum w|F_o|^2]^{1/2}$; $w = 1/[\sigma^2(F_o^2) + (0.0462P)^2 + 1.01P]$; $P = [\max(F_o^2, 0) + 2F_c^2]/3$ (all data).

at 120 °C under autogenous pressure for 4 d in a 23 mL capacity Teflon-lined stainless steel Parr hydrothermal bomb. The amounts of V, P, and $C_2O_4^{2-}$ in 5 mL of solution A are 2.4, 12.7, and 5.0 mmol, respectively. Afterward, the reactor was cooled to room temperature over a 1 d period (final pH 0.62). The product was washed with water and dried in air. Green plate crystals (92% yield based on V) were obtained as a single phase.

Compound **2** was prepared by heating 3 mL of solution A, 3 mL of water, and 0.1351 g of guanidine carbonate (0.75 mmol, Aldrich, 99%) at 140 °C for 3 d. The amounts of V, P, and $C_2O_4^{2-}$ in 3 mL of solution A are 1.4, 7.6, and 3.0 mmol, respectively. Afterward, the reactor was cooled to room temperature over 1 d (final pH 2.10). The product was washed with water and dried in air. Green plate crystals (87% yield based on V) were obtained as a single phase.

Crystal Structure. The crystal structures of **1** and **2** were determined by single-crystal X-ray diffraction methods. Preliminary examination and data collection were performed on a SMART platform diffractometer equipped with 1K CCD area detector using graphite-monochromatized Mo Kα radiation at room temperature. A hemisphere of data (1271 frames at a 5 cm detector distance) were collected using a narrow-frame method with scan widths of 0.30° in ω and an exposure time of 30 s/frame. The first 50 frames were remeasured at the end of data collection to monitor instrument and crystal stability, and the maximum correction applied to the intensities was <1%. The data were integrated using the Siemens SAINT program,[14] with the intensities corrected for the Lorentz factor, polarization, air absorption, and absorption due to variation in the path length through the detector faceplate. The program SADABS was used for the absorption correction.[15] Additional crystallographic details for **1** and **2** are described in Table 1.

The initial positions for some atoms were obtained by using direct methods. The structures were developed by using difference Fourier procedures and refined by full-matrix least-squares techniques with the use of the SHELXTL crystallographic software package.[16] For **1**, the final cycle of refinement performed on F_o^2 with 1530 unique reflections afforded residuals $R_w = 0.0791$ and $R = 0.0321$ [based on $F_o^2 > 2\sigma(F_o^2)$]. For **2**, the final cycle of refinement performed on F_o^2 with 1504 unique reflections afforded residuals $R_w = 0.1091$ and $R = 0.0449$ [based on $F_o^2 > 2\sigma(F_o^2)$]. All of the hydrogen atoms for **1** and **2** were found by a difference Fourier synthesis and refined isotropically. No unusual trends were found in the goodness of fit as a function of F_o^2, sin θ/λ, and Miller indices.

Table 2. Atomic Coordinates (×10^4) and Equivalent Isotropic Displacement Parameters (Å^2 × 10^3) for 1 and 2[a]

	x	y	z	U(eq)[a]
		1		
V	1843(1)	5742(1)	8294(1)	11(1)
P	−2785(1)	6413(1)	8790(1)	11(1)
O(1)	1465(3)	5279(3)	7981(2)	18(1)
O(2)	4694(3)	5385(3)	7897(2)	19(1)
O(3)	389(3)	3125(3)	6133(2)	16(1)
O(4)	2093(3)	3495(3)	9470(2)	19(1)
O(5)	1210(3)	7290(3)	6455(2)	18(1)
O(6)	2855(3)	7867(3)	9614(2)	21(1)
O(7)	−2298(4)	8784(3)	8609(2)	22(1)
N	−4463(5)	−1134(5)	3189(3)	27(1)
C(1)	−217(4)	3800(4)	4920(3)	13(1)
C(2)	−4504(6)	−917(5)	4800(4)	26(1)
		2		
V	3446(1)	4140(1)	8426(1)	13(1)
P	8220(2)	3665(2)	9083(1)	12(1)
O(1)	3850(5)	6527(4)	6007(3)	16(1)
O(2)	6540(5)	4749(4)	8133(4)	17(1)
O(3)	523(5)	4166(5)	7986(4)	20(1)
O(4)	2233(5)	6138(4)	9276(4)	18(1)
O(5)	4887(5)	2935(4)	6692(3)	16(1)
O(6)	3344(5)	2266(4)	9998(4)	24(1)
O(7)	8180(5)	1528(4)	9427(4)	25(1)
N(1)	12754(8)	755(8)	4049(7)	31(1)
N(2)	10817(8)	2843(6)	5206(6)	28(1)
N(3)	11616(9)	−96(7)	6846(6)	34(1)
C(1)	4695(7)	6038(6)	4803(5)	14(1)
C(2)	11737(8)	1147(7)	5379(6)	23(1)

[a] U(eq) is defined as one-third of the trace of the orthogonalized U_{ij} tensor.

Characterization. Powder X-ray data were collected on a Scintag XDS 2000 automated powder diffractometer with Cu Kα radiation ($\lambda = 1.5406$ Å) equipped with a liquid N_2 cooled germanium solid-state detector. Data were collected in the range $5° \le 2\theta \le 80°$ using $\theta-\theta$ methods in a flat-plate geometry with a horizontal stationary sample. Infrared spectra were recorded on a Mattson FTIR 5000 spectrometer within the range 800−4000 cm^{-1} using the KBr pellet method. Thermogravimetric analyses were carried out in air at a heating rate of 1°C/min, using a high-resolution TGA 2950 thermogravimetric analyzer (TA Instruments). Magnetic measurements were made with an Oxford Instruments vibrating sample magnetometer in the temperature range $4 < T$ (K) < 290 with an applied magnetic field of 1 T. A JEOL JSM-6330F scanning electron microscope and a JEOL 2000 FX transmission electron microscope were used to investigate the sample morphology.

Results and Discussion

Structures. Atom positions and selected bond lengths and angles for both compounds are given in Tables 2 and 3. The structures of **1** and **2** are isostructural with $(NH_4)_2[VO(HPO_4)]_2(C_2O_4)\cdot H_2O$ previously reported by us.[12] In **1**, each vanadium atom and phosphorus atom

(14) SAINT, Version 4.05, Siemens Analytical X-ray Instruments, Madison, WI, 1995.

(15) G. M. Sheldrick, Program SADABS, Universität Göttingen, Göttingen, Germany, 1995.

(16) G. M. Sheldrick, SHELXTL, Version 5.03, Siemens Analytical X-ray Instruments, Madison, WI, 1995.

Table 3. Selected Bond Lengths (Å) and Angles (deg) for 1 and 2

		1[a]	
V−O(6)	1.602(2)	V−O(4)	1.964(2)
V−O(1)	1.990(2)	V−O(2)	2.006(2)
V−O(5)	2.077(2)	V−O(3)	2.259(2)
P−O(1)	1.513(2)	P−O(4)#1	1.515(2)
P−O(2)#2	1.525(2)	P−O(7)	1.587(2)
O(3)−C(1)	1.241(3)	O(5)−C(1)#4	1.265(3)
N−C(2)	1.482(4)		
C(1)−C(1)#4	1.539(5)	C(2)−C(2)#5	1.520(6)
O(6)−V−O(4)	104.2(1)	O(6)−V−O(1)	100.61(9)
O(4)−V−O(1)	90.77(8)	O(6)−V−O(2)	99.93(9)
O(4)−V−O(2)	88.33(8)	O(1)−V−O(2)	159.02(8)
O(6)−V−O(5)	94.20(9)	O(4)−V−O(5)	161.55(8)
O(1)−V−O(5)	86.94(8)	O(2)−V−O(5)	87.33(8)
O(6)−V−O(3)	69.89(9)	O(4)−V−O(3)	85.84(7)
O(1)−V−O(3)	80.05(7)	O(2)−V−O(3)	78.97(7)
O(5)−V−O(3)	75.73(7)		
O(1)−P−O(2)#2	106.5(1)	O(4)#1−P−O(2)#2	113.4(1)
O(1)−P−O(4)#1	114.8(1)	O(1)−P−O(7)	107.7(1)
O(4)#1−P−O(7)	105.9(1)	O(2)#2−P−O(7)	108.3(1)
C(1)−O(3)−V	112.1(2)	P#1−O(4)−V	130.8(1)
C(1)#4−O(5)−V	118.4(2)	O(3)−C(1)−O(5)#4	126.6(2)
P−O(1)−V	132.7(1)	P#3−O(2)−V	132.5(1)
O(3)−C(1)−C(1)#4	117.7(3)	N−C(2)−C(2)#5	110.6(3)
		2[b]	
V−O(6)	1.600(3)	V−O(4)	1.965(3)
V−O(2)	2.025(3)	V−O(3)	2.024(3)
V−O(5)	2.067(3)	V−O(1)	2.247(3)
P−O(4)#1	1.511(3)	P−O(3)#2	1.515(3)
P−O(2)	1.521(3)	P−O(7)	1.590(3)
O(1)−C(1)	1.249(5)	O(5)−C(1)#4	1.258(5)
N(1)−C(2)	1.322(7)	N(2)−C(2)	1.330(6)
N(3)−C(2)	1.304(7)		
C(1)−O(5)#4	1.258(5)	C(1)−C(1)#4	1.536(8)
O(6)−V−O(4)	106.4(2)	O(6)−V−O(2)	97.4(2)
O(4)−V−O(2)	89.6(1)	O(6)−V−O(3)	100.6(2)
O(4)−V−O(3)	89.6(1)	O(2)−V−O(3)	161.5(1)
O(6)V−O(5)	96.1(2)	O(4)−V−O(5)	157.5(1)
O(2)−V-O(5)	86.3(1)	O(3)−V−O(5)	87.5(1)
O(6)−V−O(1)	171.9(1)	O(4)−V−O(1)	81.7(1)
O(2)−V−O(1)	81.5(1)	O(3)−V−O(1)	80.0(1)
O(5)−V−O(1)	75.8(1)		
O(4)#1−P−O(3)#2	113.3(2)	O(4)#1−P−O(2)	113.6(2)
O(3)#2−P−O(2)	109.0(2)	O(4)#1−P−O(7)	107.5(2)
O(3)#2−P−O(7)	104.0(2)	O(2)−P−O(7)	108.8(2)
C(1)−O(1)−V	112.8(3)	P−O(2)−V	129.8(2)
P#3−O(3)−V	133.7(2)	P#1−O(4)−V	135.1(2)
C(1)#4−O(5)−V	118.4(3)	O(1)−C(1)−O(5)#4	127.0(4)
O(1)−C(1)−C(1)#4	116.3(5)	N(3)−C(2)−N(1)	121.2(5)
N(3)−C(2)−N(2)	119.8(5)	N(1)−C(2)−N(2)	119.0(5)

[a] Symmetry transformations used to generate equivalent atoms for **1**: #1, $-x, -y+1, -z+2$; #2, $x-1, y, z$; #3, $x+1, y, z$; #4, $-x, -y+1, -z+1$; #5, $-x-1, -y, -z+1$. [b] Symmetry transformations used to generate equivalent atoms for **2**: #1, $-x+1, -y+1, -z+2$; #2, $x+1, y, z$; #3, $x-1, y, z$; #4, $-x+1, -y+1, -z+1$.

occupy one crystallographically unique position. The vanadium atom is coordinated by six oxygen atoms, forming a distorted octahedron. Three of the oxygen atoms are shared with three PO_3OH groups with typical distances ranging from 1.964(2) from 2.006(2) Å. Two of the remaining oxygen atoms are shared with a $C_2O_4^{2-}$ group with longer V−O distances of 2.077(2) and 2.259(2) Å. The remaining oxygen atom has a significantly shorter V═O bond length of 1.602(2) Å (Figure 1). Two vanadium octahedra are linked together by a $C_2O_4^{2-}$ group to form $[V_2C_2O_{12}]$ dimers. Three of the oxygen atoms in the tetrahedral PO_3OH group are shared with vanadium atoms, and the fourth oxygen atom is terminal with a long P−O distance, 1.587(2) Å, indicative of

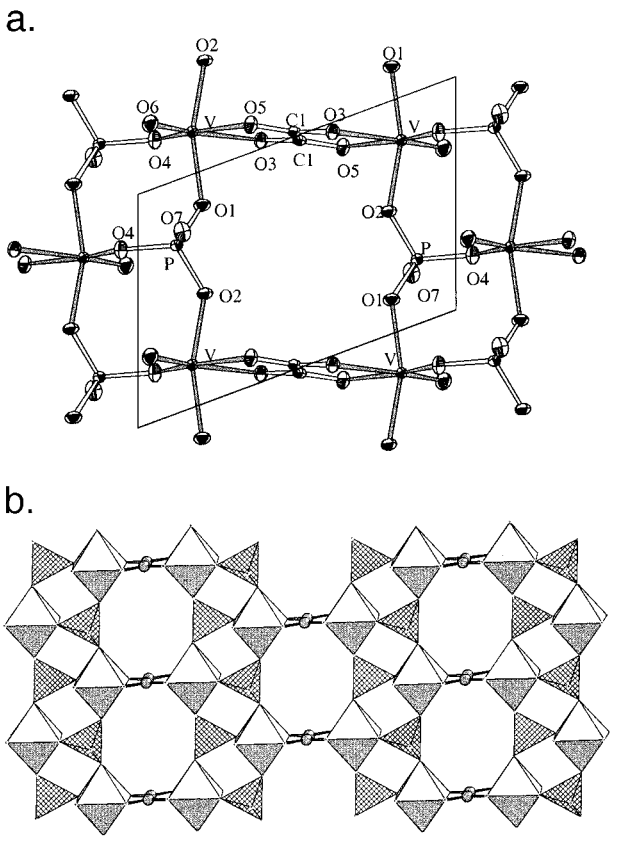

Figure 1. $[VO(HPO_4)]_2(C_2O_4)$ layer in **1**. (a) View parallel to [010]; the thermal ellipsoids are shown at 50% probability. (b) Polyhedral representation of the layer; the VO_6 and PO_4 units are shown as empty and hatched polyhedra, and carbon atoms are shown as filled circles.

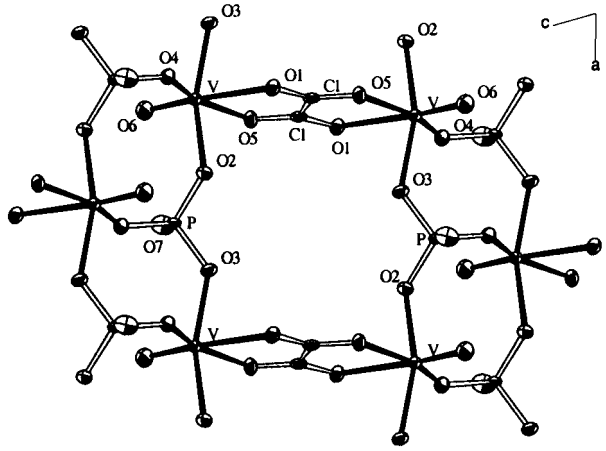

Figure 2. View parallel to [010], showing the $[VO(HPO_4)]_2(C_2O_4)$ layer connectivity in **2**. The thermal ellipsoids are shown at 50% probability.

the P−OH group. The bonding between the $[V_2C_2O_{12}]$ dimers and PO_3OH groups results in layers with composition $\{[VO(HPO_4)]_2(C_2O_4)\}^{2-}$ as shown in Figure 1. Similar $[VO(HPO_4)]_2(C_2O_4)^{2-}$ layers are found in the structure of **2** (Figure 2). The bond valence sum (BVS) values calculated for V are 4.10 and 4.05 for **1** and **2**, respectively, in good agreement with the expected value of 4.00.[17]

The $(enH_2)^{2+}$ and $(guanidiniumH)^{+}$ species are located in the space between the $[(VO(HPO_4)_2(C_2O_4)]$ layers

(17) Brese, N. E.; M. O'Keeffe, M. *Acta Crystallogr.* **1991**, *B47*, 192.

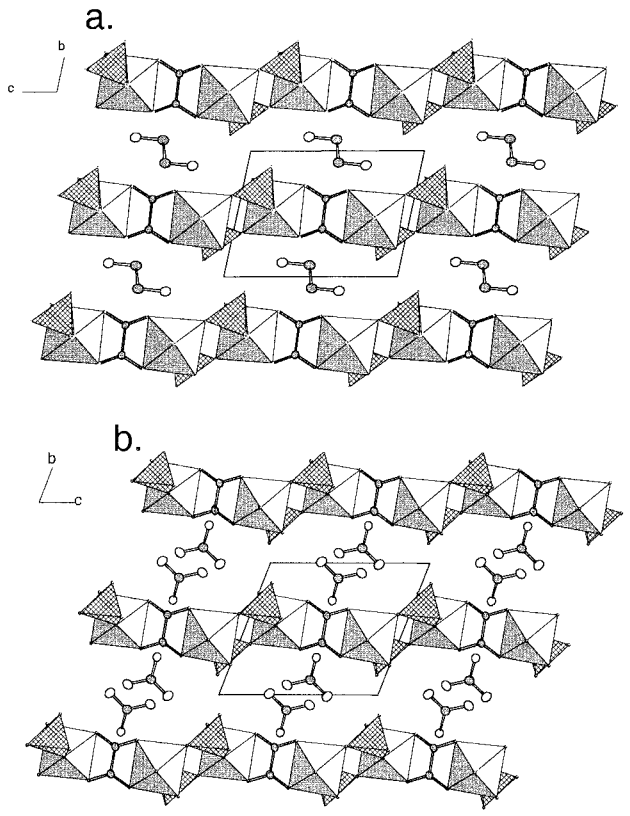

Figure 3. View parallel to [100] for the **1** (a) and **2** (b) structures. Interlayer enH_2^{2+} and $guanidiniumH^+$ cations are represented by 50% thermal ellipsoids. Polyhedra are marked as in Figure 1.

(Figure 3). The $ethylenediamineH_2$ cations are located in a $\bar{1}$ symmetry position between the $[VO(HPO_4)]_2(C_2O_4)$ layers and are H-bonded with oxygen atoms in the layers (Figure 4a). Each nitrogen atom in the ethylenediammonium cation forms H-bonds with four oxygen atoms: one terminal, O(7), atom in the PO_4 unit, two, O(3) and O(5), atoms in oxalate, and one P−O−V-bridged, O(2), atom. In **2**, the protonated guanidinium cations form H-bonds with seven neighboring oxygen atoms in the layers (Figure 4b): one terminal, O(7), atom in the PO_4 units, two, O(1) and O(5), atoms in the oxalate groups, and four V−O−P-bridged, O(2), O(3), and O(4), atoms (Figure 4b). The protonated guanidinium cations are oriented parallel to each other in the [100] direction. The distances between neighboring guanidinium cations are in the range 3.27−3.32 Å.

Double $[VO(HPO_4)]_2$ chains are present within the layers. In these double chains, the terminal P−OH groups in $VO(HPO_4)$ chains point in opposite directions, along the [100] direction in both **1** and **2** (Figures 1a and 2). A similar double $VO(HPO_4)$ chain is also found in the $VO(HPO_4)\cdot 4H_2O$ structure, which is composed of infinite $VO(HPO_4)\cdot 2H_2O$ chains containing H_2O molecules coordinated to the vanadium atom.[18,19] The double chains are also observed in the structure of $(H_2\text{-piperazine})_{0.5}VOPO_4$, where they are joined by sharing common corners to give layers of composition $[VOPO_4]$.[20,21]

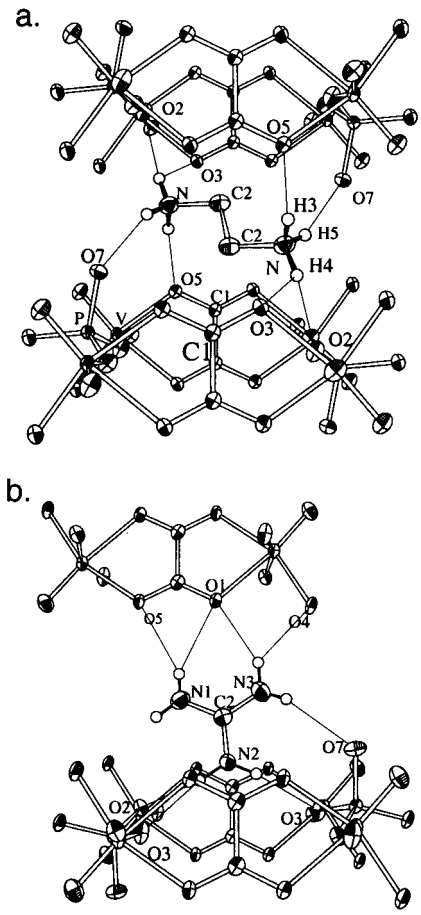

Figure 4. H-bonds between enH_2^{2+} (a) and $guanidiniumH^+$ (b) cations and oxygen atoms in the $[VO(HPO_4)]_2(C_2O_4)$ layers. The thermal ellipsoids are shown at 50% probability.

In the structures of **1** and **2**, four V atoms, two P atoms, and two oxalate species form an eight-membered ring which has a center of inversion symmetry. The size of the eight-membered ring is 5.086 Å (O(1)···O(2)) by 6.359 Å (C(1)···C(1)) and 5.107 Å (O(2)···O(3)) by 6.382 Å (C(1)···C(1)) for **1** and **2**, respectively (Figures 1a and 2).The ∠VVV angles are 92.74° and 92.53° for **1** and **2**, respectively.

The most significant differences in the structures of **1**, **2**, and $(NH_4)_2[VO(HPO_4)]_2(C_2O_4)\cdot H_2O$ are the interlayer spacings and relative shifts of adjacent layers which arise from the steric and hydrogen-bonding requirements of each of the amines. The distances between layers are 6.556, 7.239, and 7.446 Å, and the layers are shifted by 0.947, 3.132, and 7.497 Å for **1**, **2**, and $(NH_4)_2[VO(HPO_4)]_2(C_2O_4)\cdot H_2O$, respectively (Figure 3).

Characterization. The IR spectra of **1** and **2** show vibration modes for P−O, V−O, V=O, and C−O. The strongest bands (cm^{-1}) were assigned[22] as follows:

	V=O; V−O	PO_4^{3-}	$C_2O_4^{2-}$
1	964; 422, 486	1032	1672, 1385, 1317, 902
2	984; 461	941, 1032	1697, 1380, 1315, 881

The rest of the observed bands for **1** and **2** were assigned

(18) Leonowicz, M. E.; Johnson, J. W.; Brody, J. F.; Shannon, H. F., Jr.; Newsam, J. M. *J. Solid State Chem.* **1985**, *56*, 370.
(19) Fratzky, D.; Gotze, T.; Meisel, M.; Worzala, H. *Z. Kristallogr. NCS* **1999**, *214*, 9.
(20) Soghomonian, V.; Haushalter, R. C.; Chen, Q.; Zubieta, J. *Inorg. Chem.* **1994**, *33*, 1700.
(21) Riou, D.; Férey, G. *Eur. J. Solid State Inorg. Chem.* **1994**, *31*, 25.

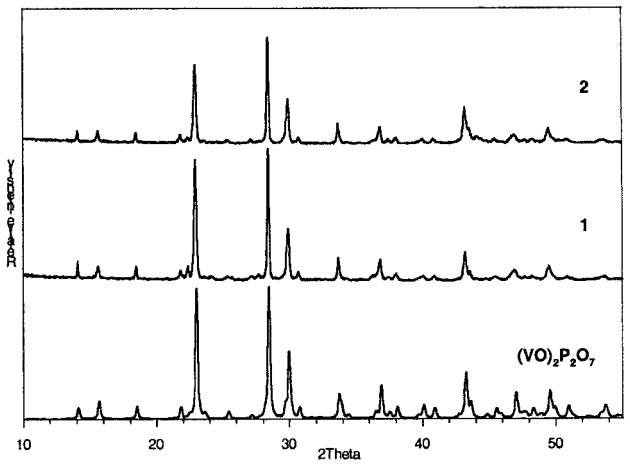

Figure 5. X-ray powder patterns of $(VO)_2P_2O_7$ after heat treatment of **1** and **2**. The lower pattern is a simulated powder pattern from the data in ref 21.

to ethylenediammonium, guanidinium cations, and water molecules, respectively.

The magnetic measurements were consistent with vanadium present as V^{4+}. At temperatures in the range $10 < T$ (K) < 290, the samples are paramagnetic and obey the Curie−Weiss law with $\mu_{eff} = 1.72$ and $1.73\ \mu_B$ for **1** and **2**, respectively, close to the value expected for $V^{4+}(3d^1,\ S = {}^1/_2,\ \mu_{eff} = 1.73\ \mu_B)$. Below 10 K, the V^{4+} magnetic moments begin to couple antiferromagnetically and the magnetic susceptibility goes through a maximum at ∼6 K.

Thermal Transformations. The thermogravimetric analysis of **1** shows that the initial weight loss at ∼350 °C is due to the loss of the elements of ethylenediammonium oxalate (weight loss calcd 31.54%, exptl 30.40%). Thus, at this temperature, ∼400 °C, the intermediate has the composition $VOHPO_4$. The evolution of the remaining proton as H_2O from the structure is complete at ∼500 °C (final weight calcd 68.06%, exptl 68.03%). At this temperature, a weight increase is observed corresponding to the partial oxidation of V^{4+} to V^{5+} due to traces of oxygen in the balance. The final product is formed as a glassy residue.

For **2**, the TGA data show that the elements of guanidinium oxalate first evolve at ∼325 °C (weight loss calcd 38.97%, exptl 39.01%), a temperature range similar to that found for the decomposition of **1**, leaving an intermediate with the composition $VOHPO_4$. The evolution of the remaining proton as H_2O from the structure is complete at ∼530 °C. Unlike **1**, no weight gain is observed and the data quantitatively confirm the conversion of $VOHPO_4$ to $(VO)_2P_2O_7$ (weight loss calcd 3.37%, exptl 3.37%).

To identify the final product after heat treatment, samples of **1** and **2** were heated in a tube furnace in N_2 gas at a heating rate of ∼50 °C/min to 700 °C. Each sample was kept at 700 °C for 5 d and then cooled to room temperature. The final gray-colored residues were analyzed by powder X-ray diffraction. The powder diffraction patterns of **1** and **2** after this treatment are identical to that of $(VO)_2P_2O_7$ as shown in Figure 5. The simulated data are based on the structure of $(VO)_2P_2O_7$ reported by Nguyen et al.[23]

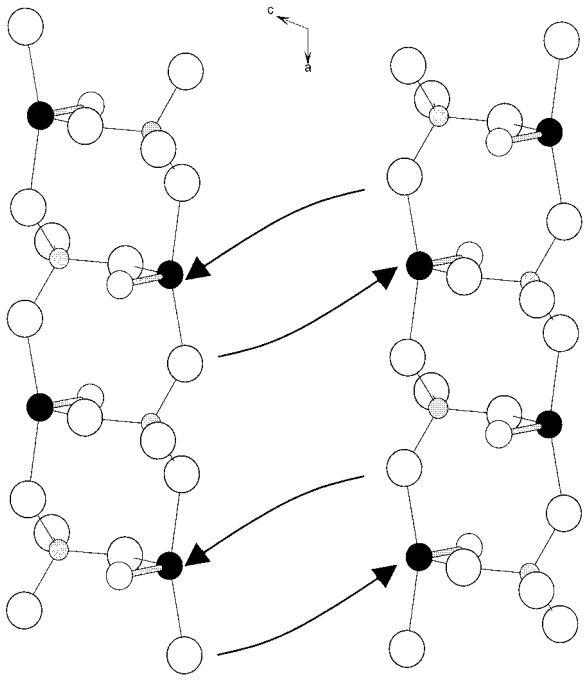

Figure 6. Proposed pathway to the intermediate $VOHPO_4$ phase in the thermal decomposition of **1** and **2**.

The overall decomposition reactions based on the weight loss data are summarized below:

$$(enH_2)[VO(HPO_4)]_2(C_2O_4) \xrightarrow{-(en + H_2C_2O_4)} 2VOHPO_4 \xrightarrow{-H_2O} (VO)_2P_2O_7$$

$$(GH)_2[VO(HPO_4)]_2(C_2O_4) \xrightarrow{-(2G + H_2C_2O_4)} 2VOHPO_4 \xrightarrow{-H_2O} (VO)_2P_2O_7$$

The structure of $(VO)_2P_2O_7$ is closely related to the structures of **1** and **2**. The unit cell of $(VO)_2P_2O_7$ is monoclinic with lattice constants $a = 7.7276(3)$ Å, $b = 16.5885(4)$ Å, $c = 9.5796(5)$ Å, and $\beta = 89.975(3)°$.[23] The VPO layers are joined together through V−O═V and P−O−P bonds, resulting in chains of vanadium octahedra sharing opposite corners and pyrophosphate groups. The structure of **1** and **2** in the *ac* plane is topologically related to that of $(VO)_2P_2O_7$ in its *bc* plane.

The structures of **1** and **2** can be transformed through several steps to give $(VO)_2P_2O_7$: removal of organoammonium cations between the layers together with removal of oxalate groups in the layers, rearrangement of the vanadium coordination environment, and condensation of vanadium and phosphate polyhedra. One possible mechanism for the transformation of the initial structure to the $VOHPO_4$ intermediate is shown in Figure 6. The $VOHPO_3$ chains are shown viewed down the crystallographic *b* axis of the starting structure, after the oxalate groups have been removed. The orientations of the V═O and PO_3OH groups are preserved when the two chains are linked by sharing the

(22) Nakamoto K. *Infrared and Raman Spectra of Inorganic and Coordination Compounds*, 5th ed.; John Wiley & Sons: New York, 1997.

(23) Nguyen, P. T.; Hoffman, R. D.; Sleight, A. W. *Mater. Res. Bull.* **1995**, *30*, 1055.

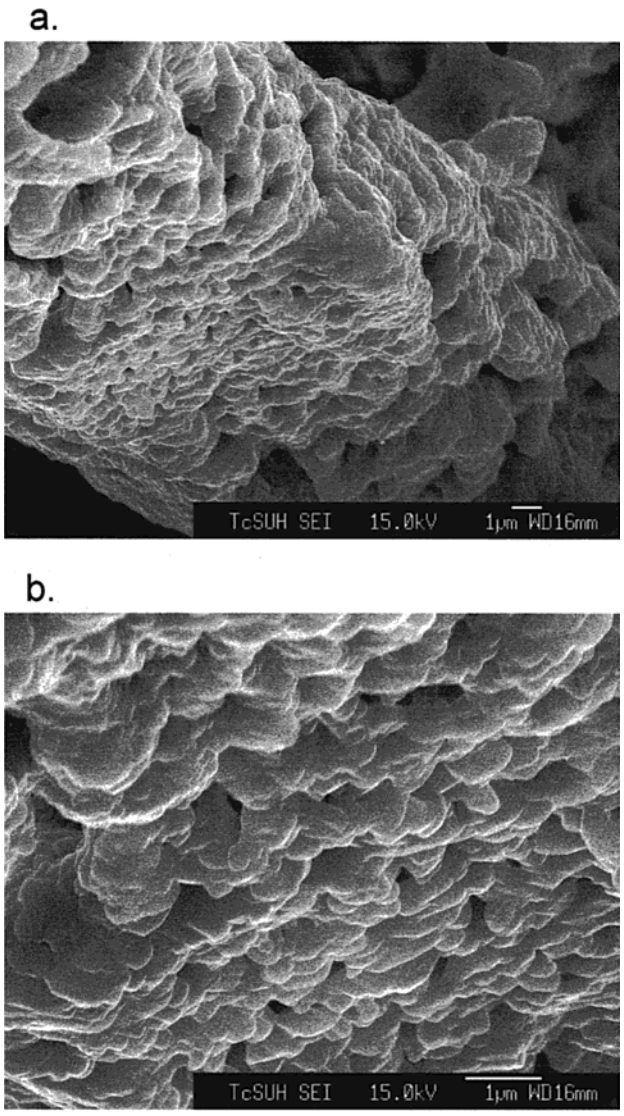

Figure 7. Scanning electron micrographs of $(VO)_2P_2O_7$ obtained by thermal treatment of **1** in N_2 at 700 °C for 5 days: (a) overall morphology of the single-crystal precursor, (b) well-packed $(VO)_2P_2O_7$ lamellae.

oxygen atoms as indicated by the arrows in Figure 6. The linking of two VO_4 units from different chains can occur in a cooperative fashion and leads to the formation of V_2O_8 dimers composed of VO_5 pyramids sharing a common edge. The bridging oxygen atoms in the dimers are also shared with phosphate oxygen atoms. The structural formula of the intermediate can be written as $VO_{1/1}O_{2/2}O_{2/3}PO_{2/2}O_{1/3}(OH)_{1/1} \equiv VOHPO_4$.

In the final step, the $VOHPO_4$ layers are cross-linked by condensation of the POH groups to form $P_2O_7^{4-}$ on elimination of H_2O and the formation of V═O—V bonds between the layers to give $(VO)_2P_2O_7$. The overall decomposition reaction involves a significant reduction in volume, and the effect of this is shown in the scanning electron micrographs in Figure 7.The overall decomposition is pseudomorphous in that the initial rod-shaped crystal morphology of the oxalatophosphate is preserved. After the decomposition, the product is highly porous and consists of small platelike crystals of $(VO)_2P_2O_7$.

A number of experiments were performed to further investigate the intermediate phase. Samples of **1** and **2** were heated in a tube furnace in flowing N_2 for reaction times varying from several hours to a month. The crystallinity varied, with samples prepared for a short time showing fewer, broader, and weaker lines than samples prepared for a long reaction time. The powder X-ray diffraction patterns of two examples of the intermediate phase are shown in Figure 8. The X-ray results for samples heated at 400 °C for 720 and 2 h are shown in parts a and b, respectively. Even after 2 h the sample shows significant crystallinity and becomes more crystalline on further annealing. The lines in the pattern after 720 h of annealing are, however, still broad but could be indexed by using the TREOR program. Two possible lattice systems were derived: tetragonal (a = 12.793 Å, c = 8.606 Å) and monoclinic (a = 13.082 Å, b = 8.634 Å, c = 6.984 Å, β = 95.944°). However, attempts to solve the crystal structure using these unit cells were not successful. The differences between the observed and calculated peak positions are somewhat larger than expected, which may suggest that neither cell is correct (Table 4).

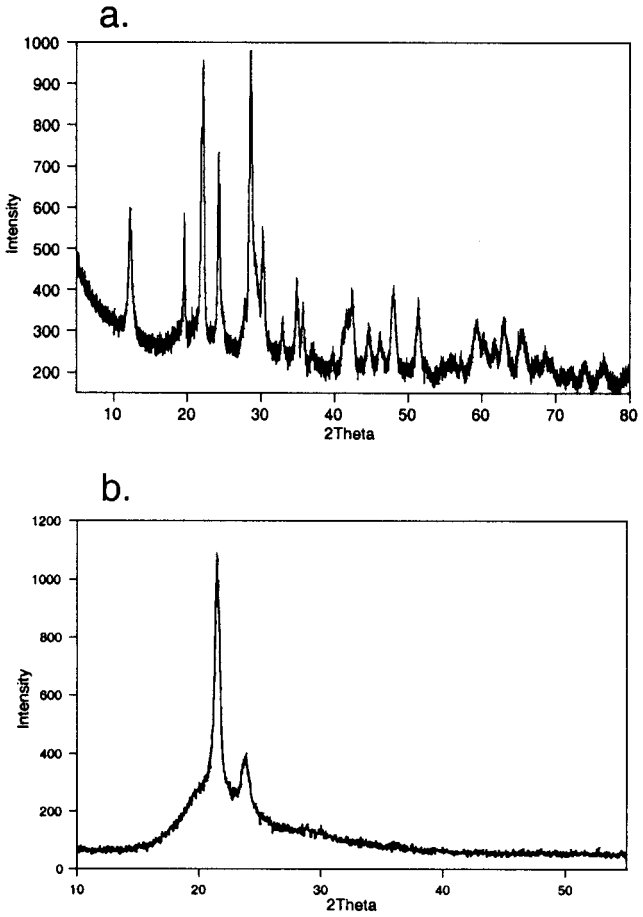

Figure 8. X-ray powder diffraction patterns of the intermediate phase obtained at 400 °C after 720 h (a) and 2 h (b).

Efforts were made to confirm the lattice parameters using electron diffraction from individual single crystals. The TEM micrographs show that the $VOHPO_4$ intermediate is composed of very thin lamellae that overlap and are folded. Electron diffraction patterns from single crystals could not be obtained because of the overlapping crystals. X-ray analysis of samples in the microscope confirmed that the V/P ratio is 1.

Finally, we note that the $VOHPO_4$ intermediate described above is structurally different from a reported

Table 4. Observed and Calculated *d* Spacings of $VOHPO_4$ Based on Monoclinic and Tetragonal Lattice Cell Parameters

		monoclinic[a]		tetragonal[b]	
2θ(obsd)	intensity	*h k l*	2θ(calcd)	*h k l*	2θ(calcd)
12.291	37	1 1 0	12.296	0 1 1	12.381
19.622	69	2 0 1	19.614	2 2 0	19.636
20.670	12	0 2 0	20.585	0 0 2	20.614
22.211	92	2 1 1	22.179	2 2 1	22.204
24.309	53	0 2 1	24.286	3 1 1	24.334
27.838	14	−2 0 2	27.814	0 4 0	27.873
28.647	100	2 2 1	28.583	2 2 2	28.619
30.306	30	2 0 2	30.394	1 3 2	30.296
32.952	9	−3 −1 2	32.955	2 4 1	32.983
34.887	17	−2 −2 2	34.853	0 4 2	34.919
35.769	14	−4 0 2	35.738	1 5 0	35.763
41.696	10	1 1 3	41.664	5 1 2	41.708
42.470	15	1 4 0	42.470	3 5 1	42.512
44.700	9	1 4 1	44.745	2 4 3	44.702
48.042	16	−4 3 2	48.084	1 6 2	48.113
51.420	13	−2 −3 3	51.460	4 4 3	51.440
59.339	10	3 0 4	59.333	8 1 1	59.312
62.976	10	−7 3 2	62.984	2 4 5	62.957

[a] Monoclinic cell parameters: $a = 13.1135$ Å, $b = 8.6222$ Å, $c = 6.9773$ Å, $\beta = 95.99°$. [b] Tetragonal cell parameters: $a = 12.7718$ Å, $c = 8.6056$ Å.

phase with the same composition. We have obtained previously a $VOHPO_4$ phase related to β-$VOPO_4$ from $VPO_4 \cdot H_2O$[24] and the structure of a similar phase was determined by Wilde et al. from powder X-ray data.[25]

(24) Vaughey, J. T.; Harrison, W. T. A.; Jacobson, A. J.; Goshorn, D. P.; Johnson, J. W. *Inorg. Chem.* **1994**, *33*, 2481.

(25) Wilde, L.; Trommer, J.; Steinike, U.; Worzala, H.; Wolf, G.-U. *Mater. Sci. Forum* **1998**, *278−281*, 704.

Conclusions

Guanidinium and ethylenediammonium vanadyl oxalatophosphates, $(C_2H_{10}N_2)[VO(HPO_4)]_2(C_2O_4)$ and $(CH_6N_3)_2[VO(HPO_4)]_2(C_2O_4)$, have been synthesized and characterized. Crystals of these compounds show a pseudomorphophic thermal transformation to vanadium pyrophosphate, $(VO)_2P_2O_7$, from rod-shaped large crystals to tiny platy crystallites. A poorly crystalline phase, $VOHPO_4$, is obtained as an intermediate during the thermal decomposition. The detailed structure of the intermediate has not been determined, but a possible mechanism for the decomposition is proposed on the basis of the structures of the end members.

Acknowledgment. This work was supported by the National Science Foundation under Grant DMR-9805881 and by the Robert A. Welch Foundation. The work made use of MRSEC/TCSUH Shared Experimental Facilities supported by the National Science Foundation under Award Number DMR-9632667 and the Texas Center for Superconductivity at the University of Houston. We thank Dr. K. Ross and Dr. I. K. Rusakova for SEM and TEM measurements.

Supporting Information Available: Tables of complete crystal data, atomic coordinates, bond distances and angles, anisotropic thermal parameters, hydrogen coordinates, and calculated and observed structure factors (PDF). This material is available free of charge via the Internet at http://pubs.acs.org.

CM010043U